Mapping Electronic Decoherence Pathways in Molecules

Ignacio Gustin,[1] Chang Woo Kim,[2] David W. McCamant,[1] and Ignacio Franco[1, 3, *]
[1] *Department of Chemistry, University of Rochester, Rochester, New York 14627, USA*
[2] *Department of Chemistry, Chonnam National University, Gwangju 61186, South Korea*
[3] *Department of Physics, University of Rochester, Rochester, New York 14627, USA*

(Dated: June 14, 2023)

Establishing the fundamental chemical principles that govern molecular electronic quantum decoherence has remained an outstanding challenge. Fundamental questions such as how solvent and intramolecular vibrations or chemical functionalization contribute to the overall electronic decoherence remain unanswered and are beyond the reach of state-of-the art theoretical and experimental approaches. Here we address this challenge by developing a strategy to isolate electronic decoherence pathways for molecular chromophores immersed in condensed phase environments that enables elucidating *how* electronic quantum coherence is lost. For this, we first identify resonant Raman spectroscopy as a general experimental method to reconstruct molecular spectral densities with full chemical complexity at room temperature, in solvent, and for fluorescent and non-fluorescent molecules. We then show how to quantitatively capture the decoherence dynamics from the spectral density and identify decoherence pathways by decomposing the overall coherence loss into contributions due to individual molecular vibrations and solvent modes. We illustrate the utility of the strategy by analyzing the electronic decoherence pathways of the DNA base thymine, its nucleoside and nucleotide in water. The electronic coherences in this case decay in ~ 30 fs. The early-time coherence loss is determined by intramolecular vibrations while the overall decay by solvent. Chemical substitution of thymine modulates the decoherence with hydrogen-bond interactions with water leading to the fastest decoherence rates. Increasing temperature leads to faster decoherence as it enhances the importance of solvent contributions but leaves the early-time decoherence dynamics intact. The developed strategy opens key opportunities to establish the connection between molecular and solvent structure and quantum decoherence as needed to develop chemical strategies to rationally modulate it.

Chemistry builds up from the idea that molecular structure determines the chemical and physical properties of matter. This principle guides the modern design of molecules for medicine, agriculture, and energy applications. However, chemical design principles have mostly remained elusive for emerging quantum technologies that exploit the fleeting but transformative properties of quantum coherence responsible for the wave-like interference of microscopic particles. Specifically, currently, it is not understood how chemical structure should be modified to rationally modulate quantum coherence and its loss. [1, 2]

To leverage Chemistry's ability to build complex molecular architectures for the development of next-generation quantum technologies, there is a critical need to identify methods to tune quantum coherences in molecules and better protect them from quantum noise (or decoherence) that arises due to uncontrollable interactions of the molecular degrees of freedom of interest with its quantum environment.[3–6] Protecting and manipulating molecular coherences is also necessary to unshackle chemical processes from the constraints of thermal Boltzmann statistics, as needed to enhance molecular function through coherence,[7] develop novel routes for the quantum control of chemical dynamics,[8, 9] and the design of optical spectroscopies with enhanced resolution capabilities.[10, 11]

In particular, electronic coherences generated by photoexcitation with ultrafast laser pulses in single-molecules and molecular arrays have received widespread attention.[12, 13] These coherences dictate the photoexcited dynamics of molecules and, as such, play a pivotal role in our elementary description of photochemistry, photophysics, charge and energy transport, and in our understanding of vital processes such as photosynthesis and vision.[14–22] These coherences decay on ultrafast (femtosecond) timescales due to the interaction of the electronic degrees of freedom with intramolecular vibrational modes and solvent.[23–26] Despite considerable experimental and theoretical efforts to study electronic decoherence in molecules,[12, 23, 24, 27–33] the basic chemical principles of electronic decoherence are still not understood. For instance, *how* does electronic coherences in, say, the DNA base thymine decohere in water? How do the different vibrations in the molecule and solvent contribute to the overall coherence loss and which one is dominant? How do chemical functionalization and isomerism influence the different contributions to the overall decoherence? Addressing these basic questions requires a general strategy to connect chemical structure of both molecule and solvent to quantum decoherence phenomena.

From an experimental perspective, the task requires a method that enables the decomposition of the overall decoherence into individual contributions by chemical groups. This is beyond what can be done using optical absorption or fluorescence,[34] photon-echo[27–

---

[*] ignacio.franco@rochester.edu

https://doi.org/10.26434/chemrxiv-2023-ld0d4 ORCID: https://orcid.org/0000-0003-0240-8782

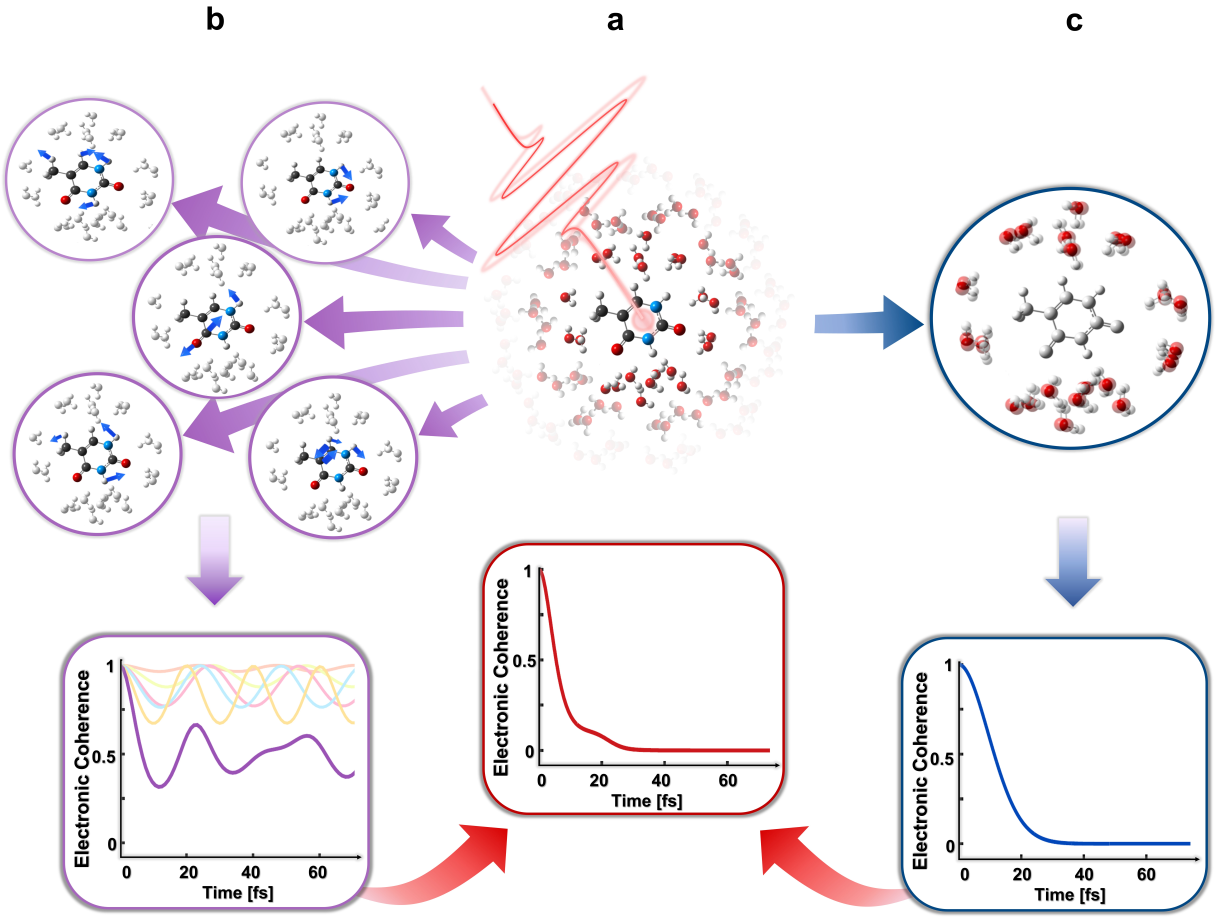

FIG. 1. **Mapping electronic decoherence pathways.** (a) Photoexcitation of molecules creates electronic superposition states with coherences that decay on ultrafast timescales due to interactions of the electronic chromophore with the surrounding nuclei (solvent and intramolecular vibrations). Here we advance a method to quantify the overall decoherence and decompose it into contributions due to specific vibrational modes (b) and solvent (c), thus establishing decoherence pathways that link chemical structure with quantum decoherence. This is done by extracting the highly structured spectral densities for solvated molecules directly from resonant Raman experiments and using the theory of decoherence functions to isolate individual contributions by solvent and vibrational modes. The strategy opens exciting opportunities to unlock the chemical principles of electronic quantum decoherence.

29] and even multidimensional laser spectroscopies.[12] To varying extents, these techniques enable characterizing the overall decoherence time scale and the molecular Hamiltonian, but do not offer means to disentangle the contributions by specific functional chemical groups.

From a theory perspective, the challenge is that accurately capturing the decoherence requires a fully-quantum quantitative description of the energetics and dynamics of the molecule in its chemical environment, and the computational cost of doing so increases exponentially with the size of the molecule and the environment. For this reason, most of our theoretical understanding of decoherence arises from model problems that, while extremely useful, do not fully capture the complexities of realistic chemical systems.[35, 36] For instance, recent efforts to quantify electronic decoherence by explicitly propagating multidimensional quantum dynamics of molecules have so far been limited to systems at zero temperature and in vacuum,[23, 26, 37–40] and thus are not informative of quantum decoherence in solvent and other condensed phase environments. In turn, efforts to include the influence of thermal environments implicitly through numerically exact quantum master equations, such as the HEOM[41, 42] and TEMPO[43], have thus far been mostly limited to simple models that do not necessarily capture the complexity of chemical environments.[44–46]

Specifically, in quantum master equations the interaction between the molecular chromophore and its thermal environment is characterized by a spectral density, $J(\omega)$[47], which quantifies the frequencies of the nuclear environment, ω, and their coupling strength with the electronic excitations. Unfortunately, the quantitative determination of $J(\omega)$ has remained elusive to theory[48–53], and its experimental characterization is limited.[54–

58] For this reason, most studies of molecular decoherence based on quantum master equations rely on simple models of spectral density that do not capture the interactions of realistic chemical problems.[44–46]

Here we introduce a general strategy to quantitatively characterize the electronic decoherence dynamics of molecules in realistic chemical environments and to map decoherence pathways, see Fig. 1. The strategy is based on reconstructing the spectral density $J(\omega)$ from resonant Raman experiments [11, 59] and decomposing the overall coherence decay into contributions by individual vibrational and solvent modes. Using this strategy, we can now address previously inaccessible questions, such as the interplay of solvent and vibrational contributions and the influence of chemical substitution on quantum decoherence. The reconstructed spectral densities open opportunities to investigate molecular decoherence dynamics in realistic chemical environments using state-of-the-art methods in quantum dynamics. Further, the overall strategy connects chemical structure to quantum decoherence dynamics and opens unique opportunities to develop the chemical principles of quantum decoherence.

Quantum coherences are usually defined as the off-diagonal elements of the density matrix $\sigma(t)$ expressed in a given basis. For molecular quantum dynamics, it is useful to think about coherences in the energy basis $\sigma_{eg}(t) = \langle e| \sigma(t) |g\rangle$ between an electronic ground $|g\rangle$ and excited state $|e\rangle$ as they lead to quantum beatings[10] that are visible in laser spectroscopies. During decoherence electronic superposition states with density matrix $\sigma = |\psi\rangle\langle\psi|$, where $|\psi\rangle = c_g |g\rangle + c_e |e\rangle$, decay to a statistical mixture of states $\sigma(t) = p_g |g\rangle \langle g| + p_e |e\rangle \langle e|$ where $p_i \geq 0$ are the state populations. This decay is ubiquitous and arises due to the interaction of the electrons with the surrounding nuclei (vibrations, torsions, and solvent).[60–62]

At zero temperature, electronic decoherence is understood as arising due to nuclear wavepacket evolution in alternative potential surfaces. [23, 30–33, 63–65] In this view, the wavefunction of electrons and their nuclear environment is in an entangled state $|\Psi(t)\rangle = |g\rangle |\chi_g(t)\rangle + |e\rangle |\chi_e(t)\rangle$, where $|\chi_n\rangle$ is the nuclear wavepacket evolving in the ground $n = g$ or excited $n = e$ potential energy surface $E_n(\mathbf{x})$ and $\{\mathbf{x}\}$ are the nuclear coordinates. In this case, the electronic coherences $\sigma_{eg}(t) = \langle \chi_e(t)| \chi_g(t)\rangle$ decay with the overlap between the nuclear wavepackets in the ground and excited state. At finite temperatures T, for early times t [24, 63, 64, 66] the electronic coherences $|\sigma_{eg}(t)|^2 = |\sigma_{eg}(0)|^2 \exp\left(-t^2/\tau_{eg}^2\right)$ decay like a Gaussian with a time scale $\tau_{eg} = \frac{\hbar}{\sqrt{\langle \delta^2 \mathcal{E}_{eg}\rangle}}$ dictated by fluctuations of the energy gap $\mathcal{E}_{eg}(\mathbf{x}) = E_e(\mathbf{x}) - E_g(\mathbf{x})$ due to thermal or quantum fluctuations of the nuclear environment. At high temperatures, $\tau_{eg} = \frac{\hbar}{\sqrt{s k_B T}}$ is simply connected to the Stokes shift s.

We first note that $J(\omega)$ can be reconstructed from resonant Raman (RR) spectroscopy as this technique provides detailed quantitative structural information about molecules in solution. While RR experiments are routinely used to investigate the vibrational structure and photodynamics of molecules[67–69], their utility for decoherence studies had not been appreciated before. A leading technique used to reconstruct $J(\omega)$ for molecules is difference fluorescence line narrowing spectra (ΔFLN).[54–58, 70] The advantage of RR over ΔFLN is that it can be used in both fluorescent and non-fluorescent molecules[71–74] (instead of only fluorescent), in solvent (instead of glass matrices), at room temperature (instead of cryogenic temperatures), and that it offers the possibility of varying the nature of the solvent and the temperature.

In RR spectroscopy, incident light E_L of frequency ω chosen to be at resonance with an electronic transition is scattered inelastically, yielding a Stokes and an anti-Stokes signal E_S that changes the molecular vibrational state. All vibrational modes that are coupled to the electronic transition yield a RR signal.[75] The theory of RR cross sections (see Supplementary Information and Refs. 11, 76–79) is based on a two-surface molecular model, with Hamiltonian $H_M = H_g |g\rangle \langle g| + H_e |e\rangle \langle e|$. Here, $H_g = \sum_\alpha \left(\frac{p_\alpha^2}{2m_\alpha} + \frac{1}{2} m_\alpha \omega_\alpha^2 x_\alpha^2\right)$ is the ground-state state nuclear Hamiltonian, where x_α and p_α are the position and momentum operators of the α-th mode of effective mass m_α and frequency ω_α. In turn, the excited potential energy surface consists of the same set of nuclear modes but displaced in conformational space, i.e., $H_e = \hbar\omega_{eg} + \sum_\alpha \left(\frac{p_\alpha^2}{2m_\alpha} + \frac{1}{2} m_\alpha \omega_\alpha^2 (x_\alpha - d_\alpha)^2\right)$ where $\hbar\omega_{eg}$ is the electronic excitation energy. The displacement along the α-th mode, d_α, determines the strength of the electron-nuclear coupling as measured by the Huang-Rhys factor $S_\alpha = \frac{1}{2\hbar} m_\alpha \omega_\alpha d_\alpha^2$ or reorganization energy $\lambda_\alpha = \hbar S_\alpha \omega_\alpha$. The overall Stokes shift s is determined by $s = 2\lambda = 2\sum_\alpha \lambda_\alpha$, where λ is the overall reorganization energy.

The RR experiments yield the frequencies of the vibrational modes $\{\omega_\alpha\}$ and also the Huang-Rhys factors S_α which are extracted by fitting the signal to the RR cross section.[11, 76–79] The analysis also yields contributions due to solvent, and other (sub 200 cm^{-1}) nuclear modes that cannot be experimentally resolved, to the overall line shape and Stokes shift which are captured by an overdamped oscillator with correlation time $\frac{1}{\Lambda}$ and reorganization energy λ_0.[80] The procedure that is routinely done to extract these parameters is detailed in the supplementary information.

This information is exactly what is needed to reconstruct the spectral density of molecules in solvent with full chemical complexity. In this case, the spectral density consists of a broad low-frequency feature $J_0(\omega)$ describing the influence of solvent and a series of discrete high-frequency peaks $J_\alpha(\omega)$ $(\alpha = 1, ..., N)$ due to interaction of the chromophore with intramolecular vibrational modes. The basic functional forms for the spectral density have been isolated through physical models in which the thermal environment is described as a collection of harmonic oscillators (the so-called Brownian oscillator model).[11] This yields,

$$J(\omega) = \sum_{\alpha=0}^{N} J_\alpha(\omega), \text{ where}$$
$$J_\alpha(\omega) = \frac{2}{\pi}\lambda_\alpha \omega_\alpha^2 \frac{\omega\gamma_\alpha}{\left(\omega_\alpha^2 - \omega^2\right)^2 + \omega^2\gamma_\alpha^2} \quad (1)$$

and $\{\gamma_\alpha^{-1}\}$ are the vibrational lifetimes. The solvent spectral density can be adequately modeled via a Drude-Lorentz functional form $J_0(\omega) = \frac{2}{\pi}\lambda_0 \frac{\omega\Lambda}{\omega^2+\Lambda^2}$ which arises from $J_\alpha(\omega)$ when the lifetimes are short (i.e. when $\omega_\alpha/\gamma_\alpha \ll 1$). Thus, all the parameters defining the spectral density can be extracted from the RR experiments. While the specific value of γ_α cannot be directly resolved using RR, its value plays no significant role in electronic decoherence as vibrational relaxation occurs on much longer time scales for physical values of $\hbar\gamma_\alpha \in (1, 20)\text{cm}^{-1}$ (See Fig. S1).[48, 81, 82]

The spectral densities that can be extracted from RR are due to "pure dephasing" processes where there is no net exchange of energy between the system and the environment. That is, for processes in which the environment does not lead to electronic transitions or relaxation. In molecules, these pure dephasing processes have been the subject of intense interest as they typically occur in time scales that are much faster than the overall relaxation and dominate the decoherence dynamics. [83, 84]

Once a spectral density is extracted from RR experiments, the task is then to use it to capture the realistic quantum dynamics of the molecular chromophore. The challenge is that the computational cost of doing so increases exponentially with the number of features $N + 1$ in the environment.

Second, we note that pure-dephasing processes occurring in thermal harmonic environments admit an exact solution without explicit propagation. In this case [60, 85, 86], the decay of the off-diagonal elements of the density matrix $|\sigma_{eg}(t)| = |\sigma_{eg}(0)| \exp[-\Gamma(t)]$ is determined by the decoherence function

$$\Gamma(t) = \frac{1}{\hbar}\int_0^\infty d\omega\, J(\omega) \coth\left(\frac{\hbar\omega}{2k_BT}\right)\frac{1-\cos(\omega t)}{\omega^2} \quad (2)$$

where k_BT is the thermal energy. Thus, computing the decoherence dynamics amounts to accurately calculating $\Gamma(t)$ via numerical integration thus avoiding explicit time propagation of $\sigma(t)$.

Third, remarkably, in this context, it is possible to extract decoherence pathways in molecules by decomposing the overall decoherence into contributions due to solvent and specific vibrational modes. Inserting Eq. (1) into Eq. (2) leads to a decomposition of the decoherence function $\Gamma(t) = \sum_{\alpha=0}^{N}\Gamma_\alpha(t)$ into individual contributions by specific nuclear modes

$$\Gamma_\alpha(t) = \frac{1}{\hbar}\int_0^\infty d\omega J_\alpha(\omega) \coth\left(\frac{\hbar\omega}{2k_BT}\right)\frac{1-\cos(\omega t)}{\omega^2}. \quad (3)$$

Alternative methods to recover the overall decoherence time such as photon-echo experiments[27–29], optical absorption cross-section[34] and even 2D electronic spectroscopy[12] cannot decompose the overall signal into contributions by solvent and specific vibrational modes. This unique aspect of our strategy opens a remarkable opportunity to develop chemical insights on decoherence dynamics by isolating contributions due to particular nuclear modes.

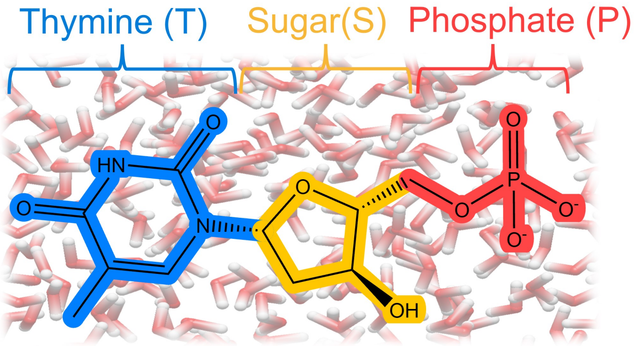

FIG. 2. **Molecular structure of DNA base thymine (T) its nucleoside (T+S) and nucleotide (T+S+P)**

To illustrate the power of the strategy, based on an RR analysis by Loppnow[87] we have reconstructed the spectral density for a DNA nucleotide (thymidine 5'-monophospate), see Fig. 2, in water at 298 K and used it to scrutinize its decoherence dynamics. Figure 3 shows the reconstructed spectral density and the overall decoherence dynamics. The parameters used to reconstruct the spectral density are listed in Table SI of the supplementary information. The spectral density (Fig. 3a) consists of a broad low-frequency feature (blue line, inset) due to solvent and several sharp peaks due to intramolecular vibrations. The overall decoherence (Fig. 3b, red line) shows an initial Gaussian decay profile, followed by a partial recurrence at $\sim$ 20 fs and a complete decay of coherence in $\sim$ 30 fs. The Gaussian feature of the decoherence is a universal feature of initially separable system-bath states [24] and can be seen as arising due to the quantum Zeno effect. The recurrence signals the partial recovery of the nuclear wavepacket overlap $|\langle\chi_e(t)|\chi_g(t)\rangle|$ due to the wavepacket dynamics in the excited state potential energy surface.[23]

To understand the role of solvent and intramolecular vibrations on the decoherence, Fig. 3b shows the contributions due to solvent (blue line), vibrations (dashed line), and solvent plus specific vibrational modes (yellow and orange lines). As shown, the early-time decoherence dynamics is dominated by vibrational contributions while the overall coherence decay is dictated by the solvent mode. Out of all vibrational modes in the molecule, we find that the mode at 1663 cm^{-1}, plays the most important role. In fact, taking into account the solvent and just three intramolecular vibrations (at 1663 cm^{-1},

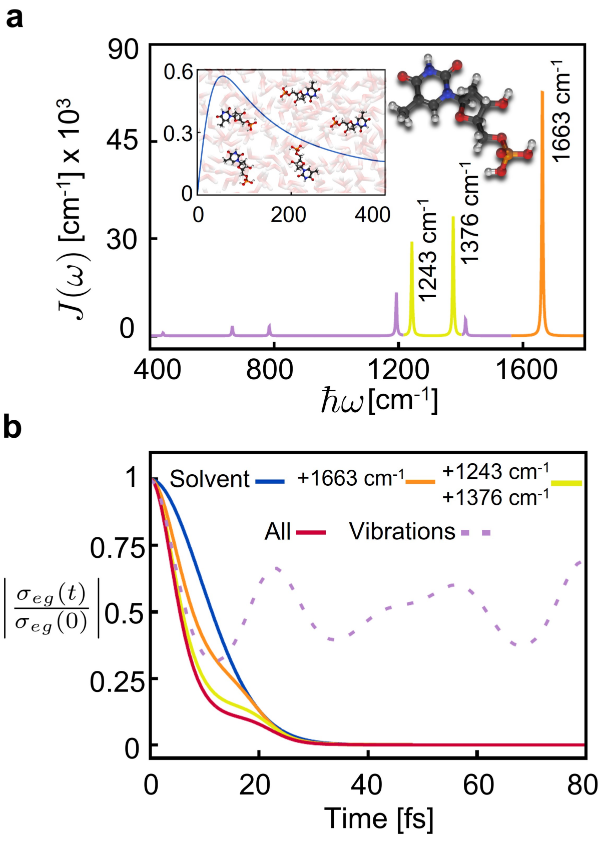

FIG. 3. **Decoherence dynamics of thymine nucleotide in water at 298 K.** (a) Spectral density $J(\omega)$ reconstructed from RR experiments in Ref. 87 with a vibrational damping factor $\hbar\gamma = 4$ cm^{-1}. (b) Electronic decoherence (red line) and its contributions due to solvent (blue line) and intramolecular vibrations (dashed line). The remaining curves depict decoherence due to solvent plus selected vibrational modes (orange: 1663 cm^{-1}; yellow: 1663 cm^{-1}+ 1376 cm^{-1}+ 1243 cm^{-1}).

1376 cm^{-1} and 1243 cm^{-1}) accounts for most of the decoherence dynamics (yellow line). Overall, these results demonstrate the close interplay between solvent and intramolecular vibrations in the decoherence dynamics.

To understand the nature of the intramolecular vibrational modes most responsible for the decoherence, we have modeled the resonance Raman spectra using time-dependent density functional theory (TD-DFT)[88–91] (computational details are included in the Supplementary Information). To keep the computations tractable, we focus on the RR spectra of thymine as the spectral features of the nucleoside and nucleotide are nearly identical.[87] Quantitative agreement between theory and experiment is obtained by including four explicit water molecules in the first solvation shell that are an active part of the vibrational motion of the molecule in its microsolvated environment.

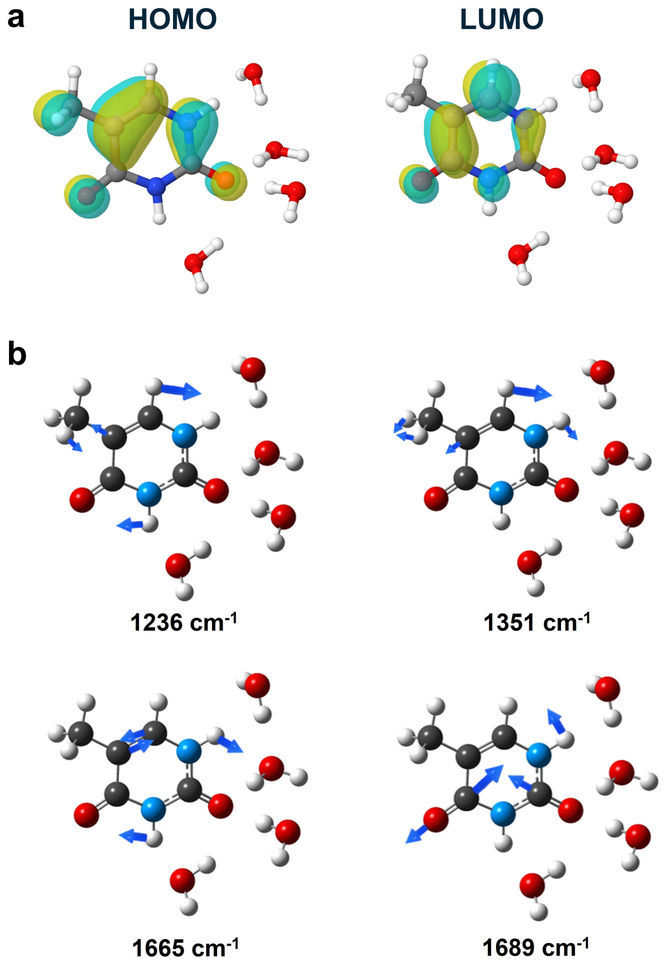

FIG. 4. **(a) Frontier molecular orbitals for thymine and (b) vibrational normal modes most important for electronic decoherence.** HOMO/LUMO stand for highest occupied/lowest unoccupied molecular orbital. The computed normal modes account to the three most prominent peaks in the spectral density in Fig. 3. The color convention is as follows: carbon (black), hydrogen (white), nitrogen (cyan) and oxygen (red).

The experimental and computed RR spectra are shown in Fig. S3. The excellent agreement between theory and experiments enables us to make vibrational assignments to all the peaks in the spectral density. Figure 4 details the frontier molecular orbitals for the electronic transition sampled by the RR experiment and the 4 normal modes responsible for the most prominent peaks in the spectral density (orange/yellow peaks in Fig. 3a). Table SVI details the computed frequencies/Huang-Rhys factors for all 75 normal modes in the complex and Fig. S4 provides an animation of the 10 normal modes most responsible for decoherence. The normal modes that contribute most importantly to the electronic decoherence are those that generate distortion around the thymine ring and/or the carbonyl bonds where the frontier orbitals involved in the electronic transition are located.

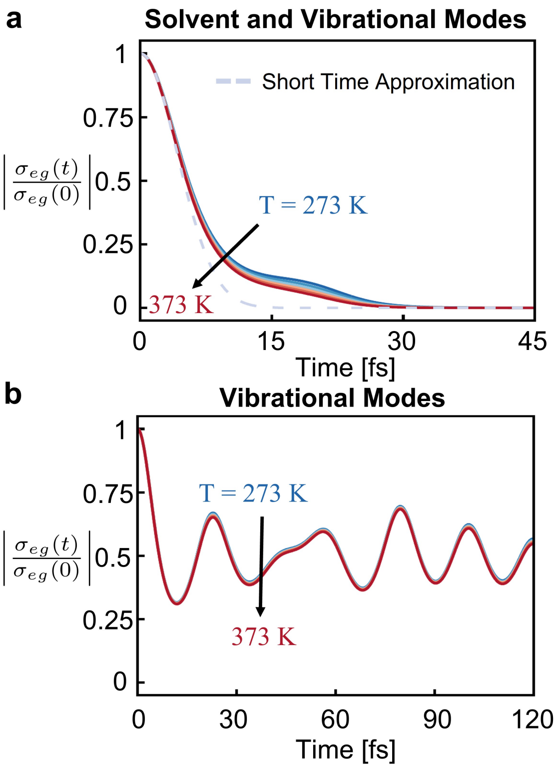

FIG. 5. **Temperature dependence of the electronic decoherence for thymine nucleotide in water.** (a) Full decoherence and (b) contributions due to vibrations only.

To understand the role of temperature in electronic decoherence, we repeated the analysis in the 273-373 K range every 10 K while assuming that $J(\omega)$ remains invariant. The results in Fig. 5 show that solvent effects become increasingly more important with temperature. In turn, the vibrational contributions (Fig. 5b) remain unaltered because thermal energy does not excite the vibrational modes that dictate decoherence. For this reason, the early-time decoherence dynamics is approximately independent of temperature as it is controlled by vibrational motion, while the overall decay is accelerated with increasing temperature leading to a reduction in the visibility of the coherence recurrence at $\sim$ 20 fs.

Recent efforts to understand electronic decoherence in molecules have focused on the influence of vibrational motion upon photoexcitation at 0 K. [23, 26, 37–40] Figures 3 and 5 show that this strategy accurately captures the early time coherence decay, which is dominated by high-frequency vibrations, but will not be able to correctly capture the overall coherence loss, which requires taking into account the solvent and the temperature dependence of the decoherence.

A useful formula for electronic decoherence time scales arises by focusing on early times, which yield a Gaussian decay $|\sigma_{eg}(t)| = |\sigma_{eg}(0)|e^{-t^2/\tau_d^2}$. [24, 30, 63] For harmonic environments, $\tau_d^{-2} = \frac{1}{2\hbar}\int_0^\infty d\omega\, J(\omega)\coth\left(\frac{\hbar\omega}{2k_BT}\right) = \frac{\hbar}{\sqrt{\langle\delta^2\mathcal{E}_{eg}\rangle}}$ as can be seen by expanding the decoherence function $\Gamma(t)$ in Eq. (2) up to second order in time. Figure 5a contrasts the exact decoherence dynamics with this Gaussian form (dashed line). As shown, this simple estimate accurately captures the early time decay but does not capture possible recurrences and overestimates the overall decoherence by a factor of $\sim$ 2. Thus, such formulas are useful to understand the early stages of decoherence but exaggerate the decoherence rate for electrons in molecules.

Nevertheless, to capture the electronic decoherence for molecules immersed in solvent and other condensed phase environments, Fig. 5 underscores the utility of the simple Gaussian estimate as it captures the early-time decoherence dynamics correctly while avoiding explicitly solving the quantum dynamics. By contrast, computationally expensive efforts to capture the decoherence based on propagating the correlated quantum dynamics of electrons and nuclei at 0 K using Multi Configurational Time Dependent Hartree (MCTDH) [26, 37, 38, 40, 92, 93] are only relevant for early times where finite temperature effects due to solvent do not play a role. Figure 5 shows that this early-time region of the decoherence can be accurately captured while avoiding propagating the quantum dynamics all together.

How does varying chemical structure influences quantum coherence loss? To address this question, we reconstructed the spectral densities of thymine (T), its nucleoside (T + sugar (S)) and nucleotide (T + S + phosphate (P)) in water at 298 K from RR data in Refs. 87 and 94. Figure 6 details the overall decoherence and the contributions of intramolecular vibrations to the decoherence in this series. The reconstructed $J(\omega)$ for thymine and its nucleoside, as well as all the needed parameters, are included in Fig. S2 and Table SII-SIII of the supplementary information, respectively.

The overall decoherence in the nucleotide is faster than in the nucleoside as the negatively charged (-2e) phosphate group increases the interactions with the surrounding water. Surprisingly, the fastest decoherence is that in thymine, even when is the least polar molecule in the set. In this case, the N-H group can strongly interact with water through hydrogen bonding.[95] Coherence recurrences are prominent in T+S because solvent-induced decoherence is the slowest in this case. By contrast, T shows no recurrences due to ultrafast decoherence due to the solvent. Figure 6b details the decoherence due to intramolecular vibrations. The trend for the early time decoherence due to vibrations is opposite to the overall behavior with T showing the slowest decoherence, followed by T+S+P and then T+S. Thus, the overall decoherence trends in Figure 6a are due to both contributions of solvent and intramolecular vibrations, even at early times.

In conclusion, we have advanced a strategy that can be used to establish the chemical principles that underlie electronic quantum coherence loss in molecules. Previously inaccessible fundamental questions such as

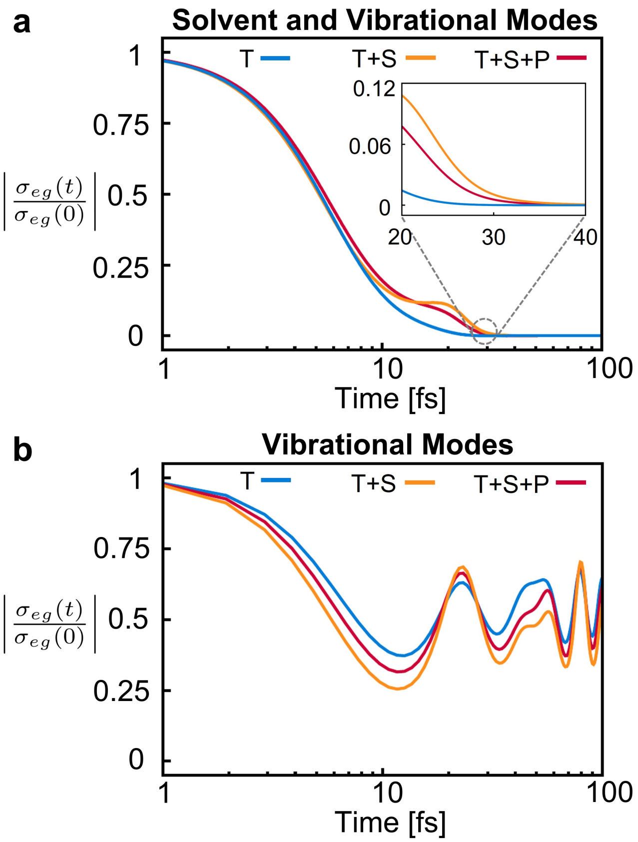

FIG. 6. **Effect of chemical substitution on electronic decoherence.** (a) Full electronic decoherence for the series (See Fig. 2). (b) Electronic decoherence due to vibrations only. Spectral densities were reconstructed from data in Ref. 87 and 94.

how chemical functionalization or solvent character contribute to the overall electronic decoherence, or how to develop chemical strategies to rationally modulate the decoherence can now be systematically addressed. The strategy is based on reconstructing spectral densities from resonant Raman experiments on molecular chromophores in solvent, and using the theory of decoherence functions to decompose the overall decoherence dynamics into contributions by individual solvent and vibrational modes, thus establishing decoherence pathways in molecules.

Using this strategy we were able to scrutinize, for the first time, the electronic decoherence dynamics of the DNA base thymine in room temperature water. In this case, the decoherence occurs in $\sim 20 - 30$ fs with the early stages dictated by intramolecular vibrations, while the overall decoherence time due to interactions with solvent. Chemical substitution of the thymine with sugar and sugar phosphate reveals a recurrence in the coherence dynamics that is suppressed by hydrogen bonding between thymine and water. The vibrational modes most responsible for the decoherence are those that distort the thymine ring and carbonyl bonds. Increasing the temperature accelerates the contributions of solvent to the decoherence but leaves the early-time decoherence dynamics intact. For pure-dephasing, this early stage of the decoherence is accurately captured by the theory of decoherence time scales [24, 63, 64, 66] which does not require propagating the quantum dynamics.

We envision the application of this strategy to elucidate the role of diverse chemical and biological environments to the decoherence, and to establish decoherence pathways for localized and delocalized, spin-specific and charge-transfer electronic excitations, and in molecules of varying size and rigidity. Further, the extracted spectral densities will be of general utility to characterize the dynamics of molecular chromophores with full chemical complexity using quantum master equations [41–43] of increasing sophistication.

ACKNOWLEDGMENTS

This work was supported by a Pump Primer II research award of the University of Rochester. I.F. is supported by the National Science Foundation under Grant No. CHE-2102386.

REFERENCES

[1] M. R. Wasielewski, M. D. Forbes, N. L. Frank, K. Kowalski, G. D. Scholes, J. Yuen-Zhou, M. A. Baldo, D. E. Freedman, R. H. Goldsmith, T. Goodson III, *et al.*, Exploiting chemistry and molecular systems for quantum information science, Nat. Rev. Chem. **4**, 490 (2020).

[2] M. Atzori and R. Sessoli, The second quantum revolution: role and challenges of molecular chemistry, J. Am. Chem. Soc. **141**, 11339 (2019).

[3] G.-Z. Zhu, D. Mitra, B. L. Augenbraun, C. E. Dickerson, M. J. Frim, G. Lao, Z. D. Lasner, A. N. Alexandrova, W. C. Campbell, J. R. Caram, *et al.*, Functionalizing aromatic compounds with optical cycling centres, Nat. Chem. **14**, 995 (2022).

[4] S. L. Bayliss, P. Deb, D. W. Laorenza, M. Onizhuk, G. Galli, D. E. Freedman, and D. D. Awschalom, Enhancing spin coherence in optically addressable molecular qubits through host-matrix control, Phys. Rev. X **12**, 031028 (2022).

[5] W. Hu, I. Gustin, T. D. Krauss, and I. Franco, Tuning and enhancing quantum coherence time scales in molecules via light-matter hybridization, J. Phys. Chem. Lett. **13**, 11503 (2022).

[6] L. Viola, E. Knill, and S. Lloyd, Dynamical decoupling of open quantum systems, Phys. Rev. Lett. **82**, 2417 (1999).

[7] G. D. Scholes, G. R. Fleming, L. X. Chen, A. Aspuru-Guzik, A. Buchleitner, D. F. Coker, G. S. Engel, R. Van Grondelle, A. Ishizaki, D. M. Jonas, *et al.*, Using coherence to enhance function in chemical and biophysical systems, Nature **543**, 647 (2017).

[8] M. Shapiro and P. Brumer, *Quantum control of molecular processes* (John Wiley & Sons, 2012).

[9] S. A. Rice, M. Zhao, *et al.*, *Optical control of molecular dynamics* (John Wiley, 2000).
[10] L. Wang, M. A. Allodi, and G. S. Engel, Quantum coherences reveal excited-state dynamics in biophysical systems, Nat. Rev. Chem. **3**, 477 (2019).
[11] S. Mukamel, *Principles of Nonlinear Optical Spectroscopy*, 6 (Oxford University Press, USA, 1995).
[12] S. Biswas, J. Kim, X. Zhang, and G. D. Scholes, Coherent two-dimensional and broadband electronic spectroscopies, Chem. Rev. **122**, 4257 (2022).
[13] R. Dani and N. Makri, Time-evolving quantum superpositions in open systems and the rich content of coherence maps, The Journal of Physical Chemistry B **126**, 9361 (2022).
[14] A. De Sio and C. Lienau, Vibronic coupling in organic semiconductors for photovoltaics, Phys. Chem. Chem. Phys. **19**, 18813 (2017).
[15] T. R. Nelson, D. Ondarse-Alvarez, N. Oldani, B. Rodriguez-Hernandez, L. Alfonso-Hernandez, J. F. Galindo, V. D. Kleiman, S. Fernandez-Alberti, A. E. Roitberg, and S. Tretiak, Coherent exciton-vibrational dynamics and energy transfer in conjugated organics, Nat. Commun. **9**, 2316 (2018).
[16] C. Kreisbeck and T. Kramer, Long-lived electronic coherence in dissipative exciton dynamics of light-harvesting complexes, J. Phys. Chem. Lett. **3**, 2828 (2012).
[17] W. Popp, M. Polkehn, R. Binder, and I. Burghardt, Coherent charge transfer exciton formation in regioregular p3ht: A quantum dynamical study, J. Phys. Chem. Lett. **10**, 3326 (2019).
[18] S. M. Blau, D. I. Bennett, C. Kreisbeck, G. D. Scholes, and A. Aspuru-Guzik, Local protein solvation drives direct down-conversion in phycobiliprotein pc645 via incoherent vibronic transport, Proc. Natl. Acad. Sci. **115**, E3342 (2018).
[19] F. C. Ramos, M. Nottoli, L. Cupellini, and B. Mennucci, The molecular mechanisms of light adaption in light-harvesting complexes of purple bacteria revealed by a multiscale modeling, Chem. Sci. **10**, 9650 (2019).
[20] S. Hahn and G. Stock, Quantum-mechanical modeling of the femtosecond isomerization in rhodopsin, J. Phys. Chem. B **104**, 1146 (2000).
[21] E. Marsili, M. H. Farag, X. Yang, L. De Vico, and M. Olivucci, Two-state, three-mode parametrization of the force field of a retinal chromophore model, J. Phys. Chem. A **123**, 1710 (2019).
[22] C. Chuang and P. Brumer, Extreme parametric sensitivity in the steady-state photoisomerization of two-dimensional model rhodopsin, J. Phys. Chem. Lett. **12**, 3618 (2021).
[23] W. Hu, B. Gu, and I. Franco, Lessons on electronic decoherence in molecules from exact modeling, J. Chem. Phys. **148**, 134304 (2018).
[24] B. Gu and I. Franco, Generalized theory for the timescale of molecular electronic decoherence in the condensed phase, J. Phys. Chem. Lett. **9**, 773 (2018), publisher: American Chemical Society.
[25] M. Vacher, M. J. Bearpark, M. A. Robb, and J. P. Malhado, Electron dynamics upon ionization of polyatomic molecules: coupling to quantum nuclear motion and decoherence, Phys. Rev. Lett. **118**, 083001 (2017).
[26] C. Arnold, O. Vendrell, and R. Santra, Electronic decoherence following photoionization: Full quantum-dynamical treatment of the influence of nuclear motion, Phys. Rev. A **95**, 033425 (2017).
[27] M. R. Salvador, M. A. Hines, and G. D. Scholes, Exciton–bath coupling and inhomogeneous broadening in the optical spectroscopy of semiconductor quantum dots, The Journal of chemical physics **118**, 9380 (2003).
[28] A. E. Colonna, X. Yang, and G. D. Scholes, Photon echo studies of biexcitons and coherences in colloidal cdse quantum dots, phys. status solidi B **242**, 990 (2005).
[29] X. Yang, T. E. Dykstra, and G. D. Scholes, Photon-echo studies of collective absorption and dynamic localization of excitation in conjugated polymers and oligomers, Phys. Rev. B **71**, 045203 (2005).
[30] H. Hwang and P. J. Rossky, An analysis of electronic dephasing in the spin-boson model, J. Chem. Phys. **120**, 11380 (2004).
[31] H. Hwang and P. J. Rossky, Electronic decoherence induced by intramolecular vibrational motions in a betaine dye molecule, J. Phys. Chem. B **108**, 6723 (2004).
[32] Y. Shu and D. G. Truhlar, Decoherence and its role in electronically nonadiabatic dynamics, J. Chem. Theory Comput. (2023).
[33] A. W. Jasper and D. G. Truhlar, Electronic decoherence time for non-born-oppenheimer trajectories, J. Chem. Phys. **123**, 064103 (2005).
[34] E. J. Heller, The semiclassical way to molecular spectroscopy, Acc. Chem. Res. **14**, 368 (1981).
[35] J. Tomasi, B. Mennucci, and R. Cammi, Quantum mechanical continuum solvation models, Chem. rev. **105**, 2999 (2005).
[36] C. Olbrich, J. Strümpfer, K. Schulten, and U. Kleinekathöfer, Theory and simulation of the environmental effects on fmo electronic transitions, J. Phys. Chem. Lett. **2**, 1771 (2011).
[37] D. Dey, A. I. Kuleff, and G. A. Worth, Quantum interference paves the way for long-lived electronic coherences, Phys. Rev. Lett. **129**, 173203 (2022).
[38] C. Arnold, O. Vendrell, R. Welsch, and R. Santra, Control of nuclear dynamics through conical intersections and electronic coherences, Phys. Rev. Lett. **120**, 123001 (2018).
[39] N. V. Golubev, T. Begušić, and J. c. v. Vaníček, On-the-fly ab initio semiclassical evaluation of electronic coherences in polyatomic molecules reveals a simple mechanism of decoherence, Phys. Rev. Lett. **125**, 083001 (2020).
[40] J. Vester, V. Despré, and A. I. Kuleff, The role of symmetric vibrational modes in the decoherence of correlation-driven charge migration, J. Chem. Phys. **158** (2023).
[41] Y. Tanimura, Numerically exact approach to open quantum dynamics: The hierarchical equations of motion (heom), J. Chem. Phys. **153**, 020901 (2020).
[42] T. Ikeda and G. D. Scholes, Generalization of the hierarchical equations of motion theory for efficient calculations with arbitrary correlation functions, J. Chem. Phys. **152**, 204101 (2020).
[43] A. Strathearn, P. Kirton, D. Kilda, J. Keeling, and B. W. Lovett, Efficient non-markovian quantum dynamics using time-evolving matrix product operators, Nat. Commun. **9**, 3322 (2018).
[44] J. Zhang, R. Borrelli, and Y. Tanimura, Proton tunneling in a two-dimensional potential energy surface with a non-linear system–bath interaction: Thermal suppression of reaction rate, J. Chem. Phys. **152**, 214114 (2020).

[45] C. Duan, C.-Y. Hsieh, J. Liu, J. Wu, and J. Cao, Unusual transport properties with noncommutative system–bath coupling operators, J. Phys. Chem. Lett. **11**, 4080 (2020).

[46] L. Varvelo, J. K. Lynd, B. Citty, O. Kühn, and D. I. Raccah, Formally exact simulations of mesoscale exciton diffusion in a light-harvesting 2 antenna nanoarray, J. Phys. Chem. Lett. **14**, 3077 (2023).

[47] A. J. Leggett, S. Chakravarty, A. T. Dorsey, M. P. A. Fisher, A. Garg, and W. Zwerger, Dynamics of the dissipative two-state system, Rev. Mod. Phys. **59**, 1 (1987).

[48] S. Maity, V. Daskalakis, M. Elstner, and U. Kleinekathöfer, Multiscale QM/MM molecular dynamics simulations of the trimeric major light-harvesting complex II, Phys. Chem. Chem. Phys. **23**, 7407 (2021).

[49] C. W. Kim, B. Choi, and Y. M. Rhee, Excited state energy fluctuations in the fenna–matthews–olson complex from molecular dynamics simulations with interpolated chromophore potentials, Phys. Chem. Chem. Phys. **20**, 3310 (2018).

[50] E. Cignoni, V. Slama, L. Cupellini, and B. Mennucci, The atomistic modeling of light-harvesting complexes from the physical models to the computational protocol, J. Chem. Phys. **156**, 120901 (2022).

[51] S. J. Jang and B. Mennucci, Delocalized excitons in natural light-harvesting complexes, Rev. Mod. Phys. **90**, 035003 (2018).

[52] M. K. Lee and D. F. Coker, Modeling electronic-nuclear interactions for excitation energy transfer processes in light-harvesting complexes, J. Phys. Chem. Lett. **7**, 3171 (2016).

[53] A. Kell, X. Feng, M. Reppert, and R. Jankowiak, On the shape of the phonon spectral density in photosynthetic complexes, J. Phys. Chem. B **117**, 7317 (2013).

[54] M. Rätsep and A. Freiberg, Electron–phonon and vibronic couplings in the FMO bacteriochlorophyll a antenna complex studied by difference fluorescence line narrowing, J. Lumin. **127**, 251 (2007).

[55] M. Rätsep, J. Pieper, K.-D. Irrgang, and A. Freiberg, Excitation wavelength-dependent electron- phonon and electron- vibrational coupling in the cp29 antenna complex of green plants, J. Phys. Chem. B **112**, 110 (2008).

[56] J. Pieper, M. Rätsep, K.-D. Irrgang, and A. Freiberg, Chromophore-chromophore and chromophore-protein interactions in monomeric light-harvesting complex II of green plants studied by spectral hole burning and fluorescence line narrowing, J. Phys. Chem. B **113**, 10870 (2009).

[57] A. Freiberg, M. Rätsep, K. Timpmann, and G. Trinkunas, Excitonic polarons in quasi-one-dimensional lh1 and lh2 bacteriochlorophyll a antenna aggregates from photosynthetic bacteria: A wavelength-dependent selective spectroscopy study, Chem. Phys. **357**, 102 (2009).

[58] G. Gryliuk, M. Rätsep, S. Hildebrandt, K.-D. Irrgang, H.-J. Eckert, and J. Pieper, Excitation energy transfer and electron-vibrational coupling in phycobiliproteins of the cyanobacterium acaryochloris marina investigated by site-selective spectroscopy, Biochim. Biophys. Acta (BBA) Bioenerg. **1837**, 1490 (2014).

[59] J. Cina, *Getting Started on Time-Resolved Molecular Spectroscopy* (OUP Oxford, 2022).

[60] H.-P. Breuer and F. Petruccione, *The Theory of Open Quantum Systems* (Oxford University Press, New York, 2002).

[61] M. A. Schlosshauer, *Decoherence: and the quantum-to-classical transition* (Springer Science & Business Media, 2007).

[62] E. Joos, H. D. Zeh, C. Kiefer, D. J. Giulini, J. Kupsch, and I.-O. Stamatescu, *Decoherence and the appearance of a classical world in quantum theory* (Springer Science & Business Media, 2013).

[63] O. V. Prezhdo and P. J. Rossky, Relationship between quantum decoherence times and solvation dynamics in condensed phase chemical systems, Phys. Rev. Lett. **81**, 5294 (1998).

[64] E. R. Bittner and P. J. Rossky, Quantum decoherence in mixed quantum-classical systems: Nonadiabatic processes, J. Chem. Phys. **103**, 8130 (1995).

[65] G. A. Fiete and E. J. Heller, Semiclassical theory of coherence and decoherence, Phys. Rev. A **68**, 022112 (2003).

[66] B. Gu and I. Franco, Quantifying early time quantum decoherence dynamics through fluctuations, J. Phys. Chem. Lett. **8**, 4289 (2017).

[67] D. R. Dietze and R. A. Mathies, Femtosecond stimulated raman spectroscopy, ChemPhysChem **17**, 1224 (2016).

[68] Z. Piontkowski, D. J. Mark, M. A. Bedics, R. P. Sabatini, M. F. Mark, M. R. Detty, and D. W. McCamant, Excited state torsional processes in chalcogenopyrylium monomethine dyes, J. Phys. Chem. A **123**, 8807 (2019).

[69] C. Fang and L. Tang, Mapping structural dynamics of proteins with femtosecond stimulated raman spectroscopy, Annu. Rev. Phys. Chem. **71**, 239 (2020).

[70] J. Pieper, M. Rätsep, I. Trostmann, F.-J. Schmitt, C. Theiss, H. Paulsen, H. Eichler, A. Freiberg, and G. Renger, Excitonic energy level structure and pigment-protein interactions in the recombinant water-soluble chlorophyll protein. II. spectral hole-burning experiments, J. Phys. Chem. B **115**, 4053 (2011).

[71] D. W. McCamant, P. Kukura, S. Yoon, and R. A. Mathies, Femtosecond broadband stimulated raman spectroscopy: Apparatus and methods, Rev. Sci. Instrum. **75**, 4971 (2004).

[72] D. W. McCamant, P. Kukura, and R. A. Mathies, Femtosecond time-resolved stimulated raman spectroscopy: Application to the ultrafast internal conversion in β-Carotene, J. Phys. Chem. A **107**, 8208 (2003).

[73] P. Kukura, D. W. McCamant, and R. A. Mathies, Femtosecond stimulated raman spectroscopy, Annu. Rev. Phys. Chem. **58**, 461 (2007).

[74] S.-Y. Lee, D. Zhang, D. W. McCamant, P. Kukura, and R. A. Mathies, Theory of femtosecond stimulated raman spectroscopy, J. Chem. Phys. **121**, 3632 (2004).

[75] J. M. Chalmers and P. R. Griffiths, *Handbook of Vibrational Spectroscopy*, Vol. 4 (Wiley, 2002).

[76] A. B. Myers, R. A. Mathies, D. J. Tannor, and E. Heller, Excited state geometry changes from preresonance raman intensities: Isoprene and hexatriene, J. Chem. Phys. **77**, 3857 (1982).

[77] A. P. Shreve and R. A. Mathies, Thermal effects in resonance raman scattering: Analysis of the raman intensities of rhodopsin and of the time-resolved raman scattering of bacteriorhodopsin, J. Phys. Chem. **99**, 7285 (1995).

[78] D. J. Tannor and E. J. Heller, Polyatomic raman scattering for general harmonic potentials, J. Chem. Phys. **77**, 202 (1982).

[79] J. B. Page and D. L. Tonks, On the separation of resonance raman scattering into orders in the time correlator

theory, J. Chem. Phys. **75**, 5694 (1981).

[80] B. Li, A. E. Johnson, S. Mukamel, and A. B. Myers, The brownian oscillator model for solvation effects in spontaneous light emission and their relationship to electron transfer, J. Am. Chem. Soc. **116**, 11039 (1994).

[81] D. I. G. Bennett, K. Amarnath, and G. R. Fleming, A structure-based model of energy transfer reveals the principles of light harvesting in photosystem ii supercomplexes, J. Am. Chem. Soc. **135**, 9164 (2013).

[82] V. I. Novoderezhkin, M. A. Palacios, H. van Amerongen, and R. van Grondelle, Energy-transfer dynamics in the lhcii complex of higher plants: Modified redfield approach, J. Phys. Chem. B **108**, 10363 (2004).

[83] D. Von der Linde, K. Sokolowski-Tinten, and J. Bialkowski, Laser-solid interaction in the femtosecond time regime, Appl. Surf. Sci. **109**, 1 (1997).

[84] D. Brinks, R. Hildner, E. M. Van Dijk, F. D. Stefani, J. B. Nieder, J. Hernando, and N. F. Van Hulst, Ultrafast dynamics of single molecules, Chem. Soc.Rev. **43**, 2476 (2014).

[85] W. G. Unruh, Maintaining coherence in quantum computers, Phys. Rev. A **51**, 992 (1995).

[86] G. M. Palma, K.-A. Suominen, and A. Ekert, Quantum computers and dissipation, Proc. R. Soc. Lond. **A452**, 567 (1996).

[87] B. E. Billinghurst, S. A. Oladepo, and G. R. Loppnow, Initial excited-state structural dynamics of thymine derivatives, J. Phys. Chem. B **116**, 10496 (2012).

[88] J. P. Perdew, M. Ernzerhof, and K. Burke, Rationale for mixing exact exchange with density functional approximations, J. Chem. Phys. **105**, 9982 (1996).

[89] S. Grimme, J. Antony, S. Ehrlich, and H. Krieg, A consistent and accurate ab initio parametrization of density functional dispersion correction (dft-d) for the 94 elements h-pu, J. Chem. Phys. **132**, 154104 (2010).

[90] D. Rappoport and F. Furche, Property-optimized gaussian basis sets for molecular response calculations, J. Chem. Phys. **133**, 134105 (2010).

[91] P. Macak, Y. Luo, and H. Ågren, Simulations of vibronic profiles in two-photon absorption, Chem. Phys. Lett. **330**, 447 (2000).

[92] U. Manthe, H. D. Meyer, and L. S. Cederbaum, Wavepacket dynamics within the multiconfiguration hartree framework: General aspects and application to nocl, J. Chem. Phys. **97**, 3199 (1992).

[93] M. H. Beck, A. Jäckle, G. A. Worth, and H.-D. Meyer, The multiconfiguration time-dependent hartree (mctdh) method: a highly efficient algorithm for propagating wavepackets, Phys. Rep. **324**, 1 (2000).

[94] S. Yarasi, P. Brost, and G. R. Loppnow, Initial excited-state structural dynamics of thymine are coincident with the expected photochemical dynamics, J. Phys. Chem. A **111**, 5130 (2007).

[95] L. Beyere, P. Arboleda, V. Monga, and G. Loppnow, The dependence of thymine and thymidine raman spectra on solvent, Can. J. Chem. **82**, 1092 (2004).